In: 2023 AIAA Aviation and Aeronautics Forum and Exposition (AIAA AVIATION Forum), 12-16 June 2023, San Diego, CA
DOI: 10.2514/6.2023-3307

Deep-Learning for Flow-Field Prediction of 3D Non-Axisymmetric Aero-Engine Nacelles

Fernando Tejero*, David MacManus†, Jesus Matesanz-Garcia‡, Luca Boscagli§ and Josep Hueso-Rebassa¶
Centre for Propulsion and Thermal Power Engineering, Cranfield University, Cranfield, MK43 0AL, UK

Christopher Sheaf‖
Installation Aerodynamics Specialist, Rolls-Royce plc

Computational fluid dynamics (CFD) methods have been widely used for the design and optimisation of complex non-linear systems. Within this context, the overall process can typically have a large computational overhead. For preliminary design studies, it is important to establish design capabilities that meet the usually conflicting requirements of rapid evaluations and accuracy. Of particular interest is the aerodynamic design of components or subsystems within the transonic range. This can pose notable challenges due to the non-linearity of this flow regime. There is a need to develop low order models for future civil aero-engine nacelle applications. The aerodynamics of compact nacelles can be sensitive to changes in geometry and operating conditions. For example within the cruise segment different flow-field characteristics may be encountered such as shock-wave boundary layer interaction or shock induced separation. As such, an important step in the successful design of these new architectures is to develop methods for fast and accurate flow-field prediction. This work studies two different metamodelling approaches for flow-field prediction of 3D non-axisymmetric nacelles. Firstly, a reduced order model based on an artificial neural network (ANN) is considered. Secondly, a low order model that combines singular value decomposition and an artificial neural network (SVD+ANN) is investigated. Across a wide geometric design space, the ANN and SVD+ANN methods have an overall uncertainty in the isentropic Mach number prediction of about 0.02. However, the ANN approach has better capabilities to predict pre-shock Mach numbers and shock-wave locations.

Nomenclature

Roman symbols

f_{max}	=	Non-dimensional axial crest location
L_{nac}	=	Nacelle length
M	=	Mach number
M_{is}	=	Isentropic Mach number
$N_{samples}$	=	number of samples
N_s	=	Number of degrees of freedom
r_{max}	=	Maximum nacelle radius
r_{hi}	=	Highlight radius
r_{if}	=	Initial radius of curvature
r_{te}	=	Trailing edge radius

*Lecturer in Propulsion Systems Design, Centre for Propulsion and Thermal Power Engineering, Cranfield University
†Head of Gas Turbine Technology Group, Centre for Propulsion and Thermal Power Engineering, Cranfield University
‡Research Fellow in Propulsion Aerodynamics, Centre for Propulsion and Thermal Power Engineering, Cranfield University
§Research Fellow in Propulsion Aerodynamics, Centre for Propulsion and Thermal Power Engineering, Cranfield University
¶Research Fellow in Propulsion Aerodynamics, Centre for Propulsion and Thermal Power Engineering, Cranfield University
‖Installation Aerodynamics, Rolls-Royce plc, Derby, DE24 8BJ, UK

Published by AIAA. This is the Author Accepted Manuscript issued with: Creative Commons Attribution Non-Commercial License (CC:BY:NC 4.0).
The final published version (version of record) is available online at DOI:10.2514/6.2023-3307. Please refer to any applicable publisher terms of use

Greek symbols

ϕ	=	Nacelle azimuthal angle
β_{nac}	=	Nacelle boat-tail angle

Acronyms

ANN	=	Artificial Neural Network
DoF	=	Degree of Freedom
$iCST$	=	intuitive Class-Shape Transformation
LE	=	Leading Edge
$MFCR$	=	Mass Flow Capture Ratio
POD	=	Proper Orthogonal Decomposition
RSM	=	Response Surface Model
SVD	=	Singular Value Decomposition
TE	=	Trailing Edge

I. Introduction

Recent advances in machine learning are enabling the development of low order models for complex non-linear systems. This encompasses state-of-the-art methods for dimensionality reduction [1], multi-fidelity [2], or supervised and unsupervised learning approaches [3]. These have been used in different optimisation studies for aerodynamic applications such as airfoils [4], wings [5] or turbomachinery [6]. Within the context of a preliminary design phase, response surface models (RSMs) can be used to accelerate the overall process. The prediction capabilities of RSMs are usually limited to regression-type functions and typically focus on integral parameters, e.g. lift or drag. Whilst this is sometimes sufficient to drive the design process, these approaches lack the detailed aerodynamic characteristics of the configurations, such as the isentropic Mach number distribution across the surfaces. This is a clear drawback for multidisciplinary applications in which, for example, aerodynamic and aero-structural considerations should be taken into account. For this reason, low order models for flow-field prediction are required for complex and multidisciplinary aerodynamic systems. Sabater *et al.* [7] investigated different methods for the rapid prediction of aircraft aerodynamics using deep-learning techniques. Overall three data-driven methods were considered: Gaussian Process, proper orthogonal decomposition combined with a thin-plate spline interpolation technique [8] and deep neural networks. The three approaches were initially used for the prediction of surface pressure distribution in a 2D airfoil and the NASA CRM model. For both cases the input degrees of freedom (DoF) were the Mach number and angle of attack. It was concluded that whilst all methods were able to predict the flow-field distribution under subsonic conditions, the deep neural network was the best able to capture the shock-wave location and strength under transonic conditions. The same conclusion was derived for a third test case with the NASA CRM and 2 aerodynamic and 4 geometric DoFs. Qamar and Sanghi [9] coupled the proper orthogonal decomposition (POD) approach with a marching extrapolation procedure [10] to enable the flow-field prediction of cases that are outside of the range of the ensambling interval. The method was used for a supersonic axisymmetric surface-mounted triangular protuberance, with one aerodynamic and one geometric DoF. Relative to a direct POD extrapolation procedure, the method reduced the relative root mean square error by 50%. Li and Zhang [11] investigated the expected flow-field reconstruction accuracy on a 2D airfoil by means of POD. Whilst for a subsonic case with M = 0.5 only one POD mode was required to capture the 99% of the energy content, a total of 9 modes were needed for a transonic case with a Mach number of 0.80.

Within the context of future civil aero-engines, the trend is to increase the bypass ratio (BPR) to reduce the engine specific fuel consumption (SFC) and to improve the propulsive efficiency [12, 13]. This may lead to an increase in fan diameter which will result in a concomitant increment in the nacelle drag. For this reason, research in recent years has focused on the design and optimisation of compact nacelles for future turbofans [14–17]. Previous studies investigated the impact of bulk parameters such as nacelle length or highlight radius on the nacelle drag characteristics [14], assessed the sensitivity of compact nacelle architectures to off-design conditions [15], coupled the nacelle design process with the thermodynamic engine cycle [16] or investigated the drag reduction benefits of transonic axisymmetric natural laminar flow nacelles [17]. All these investigations were based on computationally expensive numerical simulations that are not feasible within a preliminary design stage. There is very limited information in the open literature that considers the nacelle design process with low order models [18–23]. This is caused by the large non-linearity associated to compact aero-engine nacelles at transonic conditions, and the difficulties to build accurate and reliable metamodels. Previous research has mainly focused in building surrogate models for the prediction of nacelle drag. Heidebrecht and MacManus [18] developed a low order model for a relatively large design space that contained short and long nacelle

shapes. This was achieved by generating a set of surrogate models that decomposed the problem in different Kriging processes. The overall method had a standard error for the prediction of mid-cruise drag of 3.6%. Other studies have also considered low order models for nacelle optimisation purposes [19–21]. For example, Yao *et al.* [21] developed an adaptive-surrogate-based optimization method for aero-engine nacelles. It was used for nacelle shape optimization at mid-cruise conditions with M = 0.85. Relative to a baseline, the process yielded a new configuration with a drag reduction of approximately 10%. Tejero *et al.* [22] recently demonstrated the capabilities of artificial neural networks for the prediction of nacelle drag and isentropic Mach number along 2D axisymmetric aero-engine nacelles.

Aerodynamic shape optimisation is a multidisciplinary discipline where different considerations, e.g aerodynamic or aero-structural, should be taken into account. Within the context of preliminary nacelle design, the process has been typically driven by low order models to predict the drag response of candidate configurations. However, existing capabilities are usually unable to predict the associated flow-field characteristics. The novelty of this paper is in the development of a set of surrogate-based models for the prediction of the flow-field characteristics for 3D non-axisymmetric aero-engine nacelles at transonic conditions. In this respect, two different approaches are considered. Whilst the first method is based on artificial neural networks (ANN), the second approach combines singular value decomposition (SVD) and ANNs.

II. Methodology

The CFD data used to build low order models for flow-field prediction of 3D non-axisymmetric aero-engine nacelles is generated with the approach developed by Tejero *et al.* [14, 24, 25]. A thorough description of this computational method was provided in the past [14, 24, 25], and as such, a brief overview is presented below. The nacelle shape is defined with a parametric definition using intuitive Class-Shape Transformation (iCST) [26, 27]. Each nacelle aero-line is controlled with 7 intuitive parameters: r_{hi}, L_{nac}, r_{te}, r_{if}, f_{max}, r_{max} and β_{nac} (Figure 1a). The 3D non-axisymmetric aero-engine nacelle is obtained with an azimuthal variation of the constraints applied to the 2D aero-lines. This azimuthal variation is also described with an iCST, and a total of 5 aero-lines are used to define the 3D shape ($\psi = 0^o$, 45^o, 90^o, 135^o and 180^o in Figure 1b). During the nacelle design process the variables of r_{hi}, L_{nac} and r_{te} are usually fixed and the remaining ones, i.e. r_{if}, f_{max}, r_{max} and β_{nac}, vary. As such, a total of 20 intuitive variables change during the nacelle design process [28, 29] (Figures 1a and 1b)

The computational domain is generated with a fully multi-block structured approach (Figure 1c). The compressible steady Favre-averaged Navier-Stokes equations are solved with a density-based solver [30], a second order spatial discretization and the Green-Gauss node based scheme. The turbulence closure is the k-ω SST model [31]. The first cell height is adjusted to fulfil $y^+ \approx 50$. Ideal gas properties are used and the viscosity is calculated with Sutherland's law. The farfield boundary condition is a pressure farfield in which the Mach number, static pressure and static temperature are imposed. No-slip adiabatic walls are used for all the housing component surfaces, i.e. intake, fancowl, spinner, bypass duct and core duct. The fan face is defined with a pressure outlet boundary condition in which a target mass flow is specified. This is derived from the user-prescribed mass flow capture ratio (MFCR). The bypass and core duct inlets are modelled with a pressure inlet BC in which is prescribed the total pressure and temperature. These are derived from the analysis of a thermodynamic engine cycle. The nacelles are left-right symmetric and, therefore, a symmetry plane is used to model half of the powerplant and save computational efforts. The farfield is located at $80r_{max}$ based on a previous domain sensitivity study. A grid convergence study was carried out for the proposed computational approach in which three mesh levels consisting of 0.5M, 1M and 2M were considered. For typical mid-cruise conditions, the grid convergence index (GCI) of the medium grid was 0.2% on normalised nacelle drag. As such, the mesh with 1M was selected for this study. The described computational approach for 3D non-axisymmetric nacelles was previously validated with experimental data [14]. For a nominal Mach number of 0.85, the normalised nacelle drag obtained with CFD is overpredicted by 1.1% with respect to the measurements.

The databases generated to build response surface models (RSM) for flow-field prediction were compiled with a design space exploration based on a Latin hypercube sampling [32]. This sampling technique was chosen on the basis of efficiently covering the relatively large dimensional space with 20 degrees of freedom . Two different methods are considered for the flow-field prediction of 3D non-axisymmetric aero-engine nacelles. They are based on artificial neural networks (Section II.A) and a combination of singular value decomposition and artificial neural networks (Section II.B)

A. Artificial neural network for flow-field prediction

A feed-forward artificial neural network (ANN) is used to predict the nacelle aerodynamic characteristics of 3D non-axisymmetric configurations (Figure 2). The initial layer of the ANN is composed of 20 neurons, which correspond

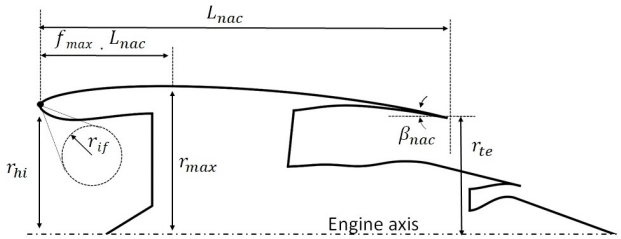

(a) 2D axisymmetric definition

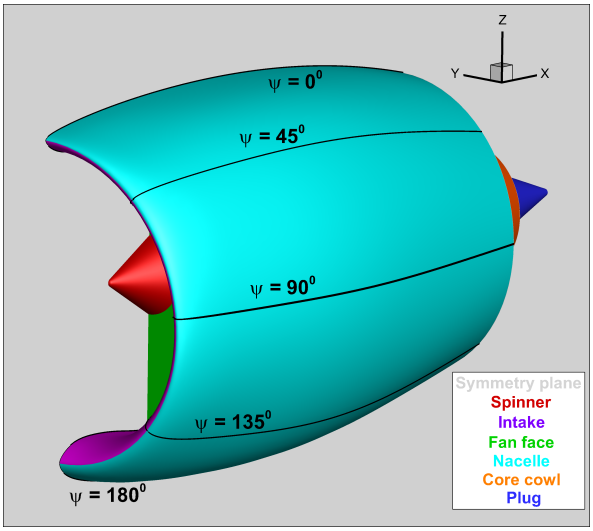

(b) 3D non-axisymmetric definition

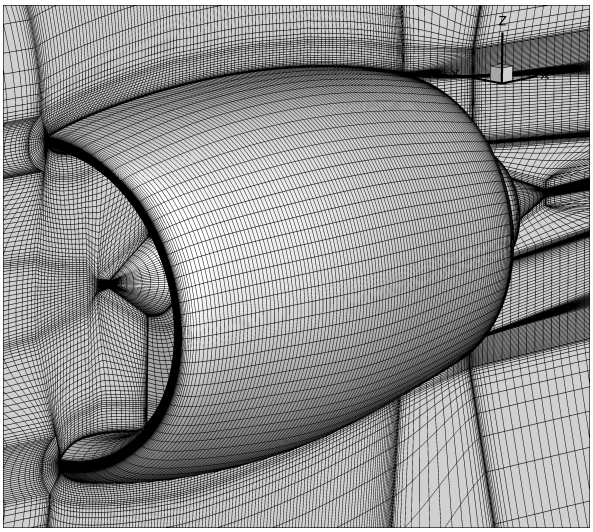

(c) Computational mesh

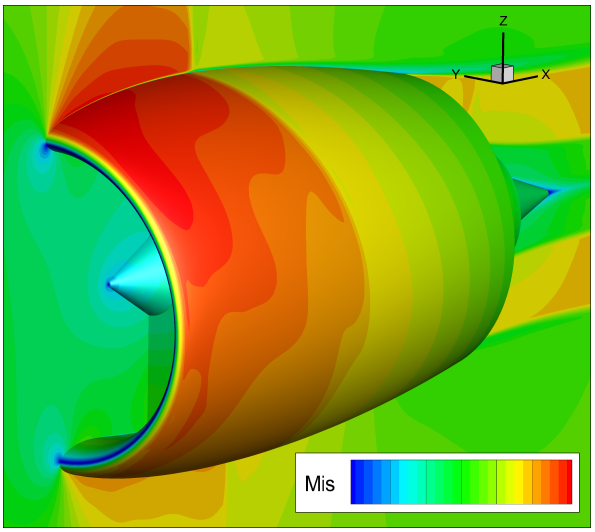

(d) CFD solution

Fig. 1 Overview of the CFD workflow for aero-engine nacelles

to the intuitive degrees of freedom (DoF) that define the 3D geometry (Figure 1). The output layer provides the predicted M_{is} value along the nacelle surface. For this study the nacelle surface has been discretized with 1850 points in which 37 equidistant points are used in the azimuthal direction, i.e. azimuthal resolution of 5^o, and 50 equidistant points are used in the axial direction. The input and output layers are connected through the hidden layers. They are used to improve the ANN prediction of the flow-field for a given training dataset. Three main hyperparameters were considered during the optimisation of the ANN architecture to minimise the uncertainty of the prediction. These were the number of hidden layers (j), neurons per layer (k) and activation function. Overall, three activation functions were investigated: sigmoid, the hyperbolic tangent (tanh), and the rectified linear unit (ReLu) (Table 1). A full factorial combination of the hyperparameters presented in Table 2 was performed during the training process of the different metamodels. The root mean squared error (RMSE) of the isentropic Mach number (M_{is}) prediction (Eq. 1) was used as the loss function during the training process. The Adaptive Moment estimation optimizer (Adam) is applied for this purpose.

Artifical Neural Network activation functions	
Name	**Activation function**
tanh	$\frac{e^z - e^{-z}}{e^z + e^{-z}}$
sigmoid	$\frac{1}{1+e^{-z}}$
ReLu	z if $z > 0$ 0 if $z <= 0$

Table 1 Summary of the activation functions used for the cells of the Neural Network

Hyperparameter	Value
Neurons	8, 16, 32, 64, 128, 256
Hidden layers	1, 2, 3, 4, 5
Activation functions	ReLu, sigmoid, tanh

Table 2 Neural network hyperparameters considered

$$RMSE = \sqrt{\frac{\Sigma_{i=1}^{N} \left(M_{is-ANN,i} - M_{is-CFD,i}\right)^2}{N}} \tag{1}$$

B. singular value decomposition and artificial neural network for flow-field prediction

A second method for flow-field prediction was investigated in this work. It combines singular value decomposition and artificial neural networks (SVD+ANN). Once the training set is compiled, the process starts with arranging the data in a matrix as a series of snapshots (Eq. 2):

$$\mathbf{M} = \begin{pmatrix} M_{1,1} & \cdots & M_{1,n} \\ \cdots & & \ldots \\ M_{m,1} & \cdots & M_{m,n} \end{pmatrix} \tag{2}$$

where m is the number of data points of the snapshot and n is the total number of snapshots that were gathered in the design space exploration. For this study, the variable m was fixed to 1850 (Section II.A). Once the matrix $\mathbf{M}$ is built, it is decomposed into the product of three matrices ($\mathbf{U}$ Σ and $\mathbf{V}^*$) by applying the singular value decomposition method (Eq. 3).

$$\mathbf{M} = \mathbf{U}\Sigma\mathbf{V}^* \tag{3}$$

where $\mathbf{U}$ is an $m \times m$ unitary matrix, Σ is an $m \times n$ rectangular diagonal matrix with non-negative real numbers on the diagonal, $\mathbf{V}$ is an $n \times n$ complex unitary matrix, and $\mathbf{V}^*$ is the conjugate transpose of $\mathbf{V}$.

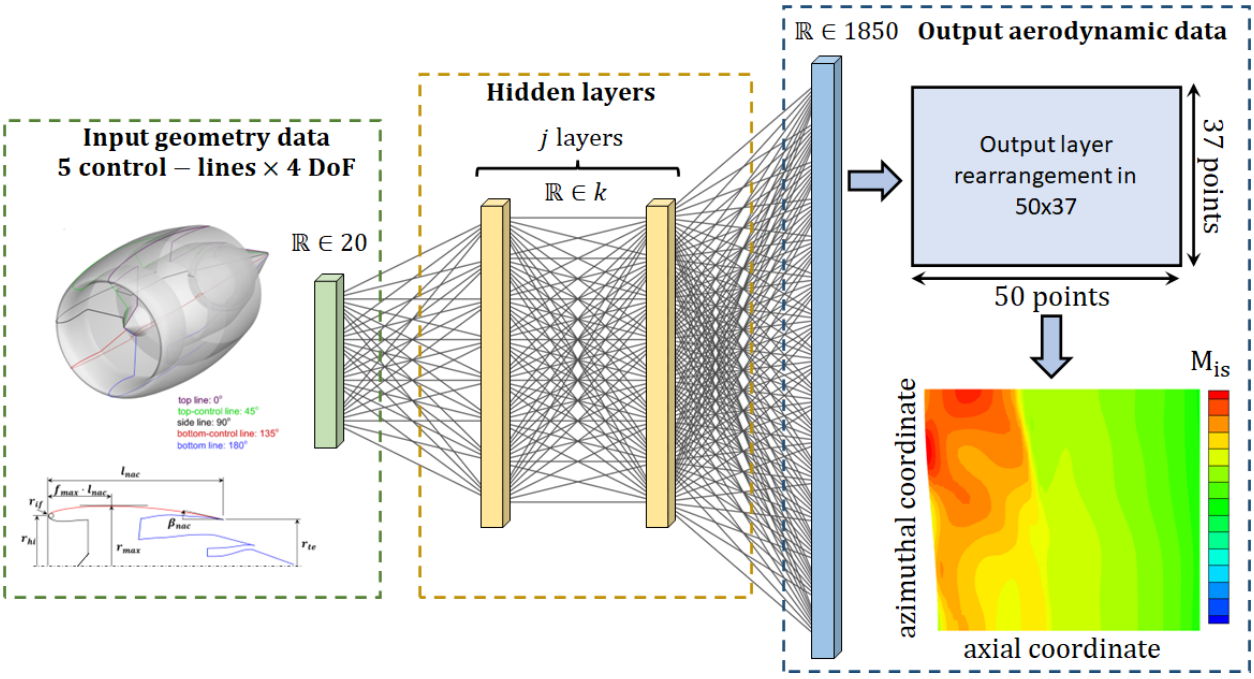

Fig. 2 Artificial neural network (ANN) for flow-field prediction of 3D non-axisymmetric aero-engine nacelles

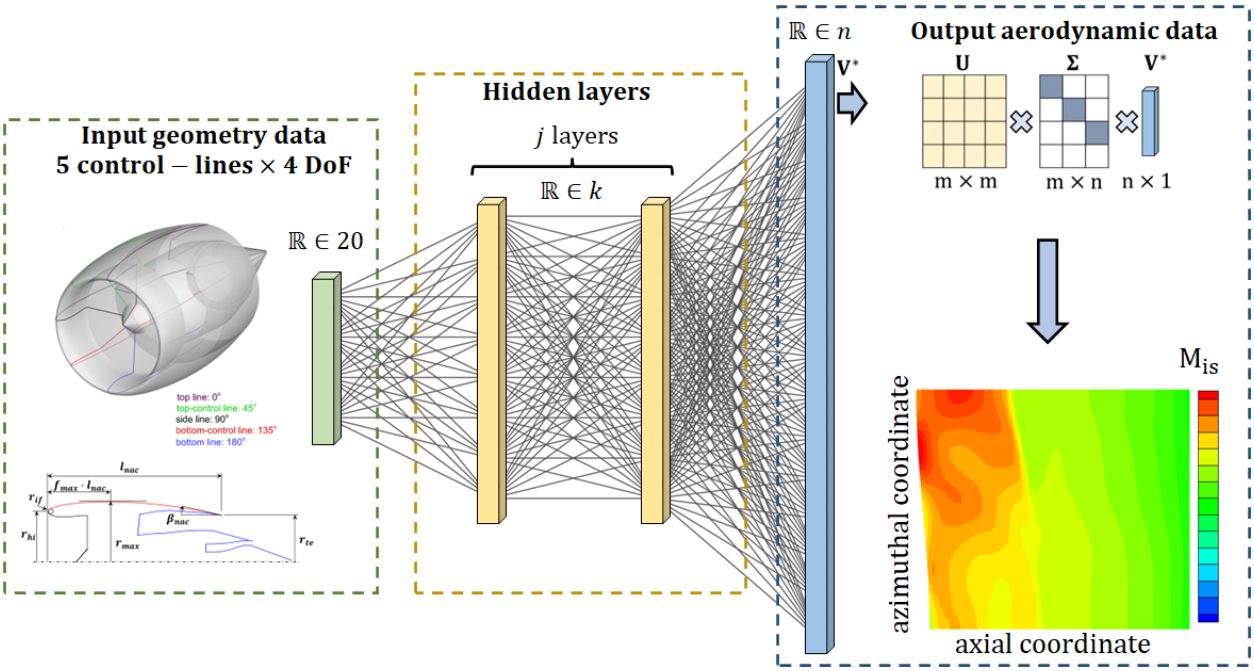

Fig. 3 singular value decomposition and artificial neural network (SVD+ANN) for flow-field prediction of 3D non-axisymmetric aero-engine nacelles

With the above decomposition, a snapshot that was contained in the database can be exactly reconstructed if all the eigenvalues of the matrix Σ are used. As the dimensionality of the problem is reduced by reducing the number of eigenvalues, larger errors in the flow-field reconstruction are obtained [9]. As such, it is required to find an acceptable

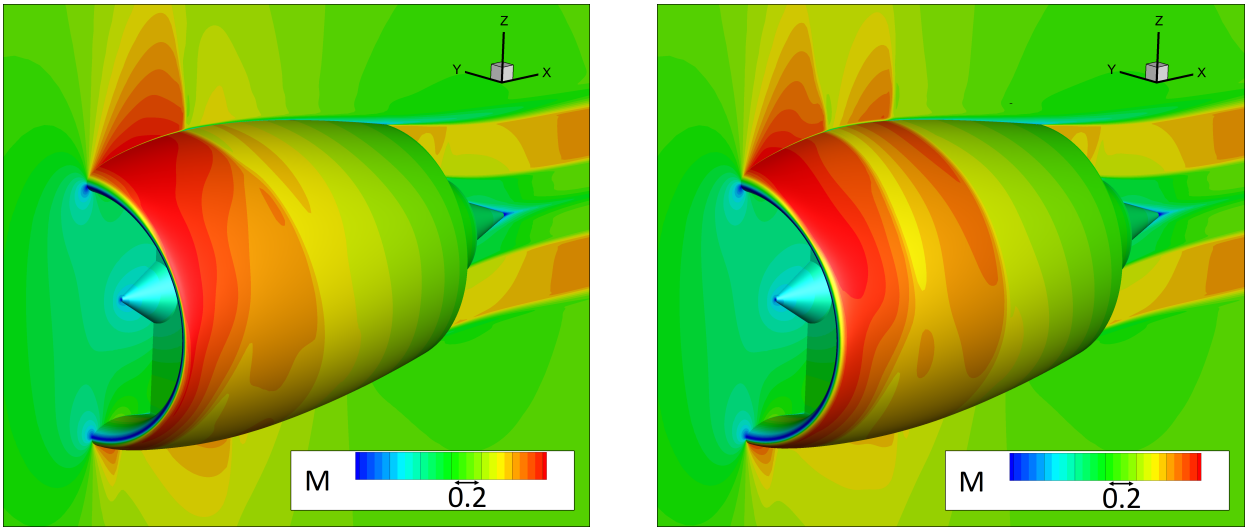

(a) Nacelle 1 **(b) Nacelle 2**

Fig. 4 Nacelle aerodynamics for 2 samples in the training dataset. Symmetry plane is colored with Mach number and the walls with isentropic Mach number

trade-off between accuracy and overall dimensionality. It is important to note that with the current form of the matrices $\mathbf{U}, \Sigma$ and $\mathbf{V}^*$, the method can only be used for data compression of the snapshots collected in the design space exploration. Whilst the matrix $\mathbf{U}$ and Σ are a generalised representation across the design space, the matrix $\mathbf{V}^*$ can be interpreted as a set of coefficients that are related to the different inputs of the database. As such, every design has associated an array of n coefficients. This dimensionality can be reduced to s, where s refers to the number of eigenvalues that are chosen in the matrix Σ. This number is usually based on the required accumulative energy of the eigenvalues [9]. Since every input has associated an s-dimensional array, an RSM can be built to model it. This enables its generalisation across all the design space. Relative to the method described in Section II.A, the main benefit of using a combination of SVD and low order models is that the RSM outputs are an array of s which is usually much lower than the original array of n. This can result in a significant time reduction in the training process and in the complexity of the deep learning architecture. For this study, the RSM to model the matrix $\mathbf{V}^*$ was an ANN. The same hyperparameters as summarized in Table 2 were used during the training process of the artificial neural network. Figure 3 shows a summary of the method for flow-field prediction by combining singular value decomposition and artificial neural networks (SVD+ANN).

III. Results

This work investigates the design space for compact aero-engine nacelle with L_{nac}/r_{hi} = 3.1. This is a short configuration that is expected for future turbofan architectures [14]. Previous studies have highlighted the large aerodynamic non-linearity of this design space [33]. As such, it represents a significant challenge for flow-field prediction with low order models. The aerodynamic analysis is carried out for a typical mid-cruise condition of long-range applications with M = 0.85 and MFCR $\approx$ 0.7.

As previously discussed, the 3D nacelle shape is defined with N_s = 20 degrees of freedom (Section II). A design space exploration, based on a Latin hypercube sampling, was performed with a total number of samples $N_{samples}$ = 2,000. This provides a ratio between the size of the database and the inputs of $N_{samples}/N_s$ = 100. A validation database was generated with a total number of samples of $N_{samples}$ = 400 to assess the predictive accuracy of the developed metamodels. To provide an initial insight of the different flow-fields that are expected in the considered design space, Figure 4 presents the transonic characteristics of two different configurations. The first nacelle has a large acceleration around the nacelle lip on the top-line, which terminates in a a well-defined shock wave at the crest (Figure 4a). The intensity of the shock gradually reduces as the azimuthal angle moves towards the bottom-line. The second nacelle has a different flow topology (Figure 4b). For the top line, there is an initial acceleration around the nacelle lip to terminate in a shock on the forebody. Then the flow reaccelerates again to a second shock wave on the afterbody.

Whilst the present study is focused in 3D non-axisymmetric configurations, a key aspect is to predict the flow-field

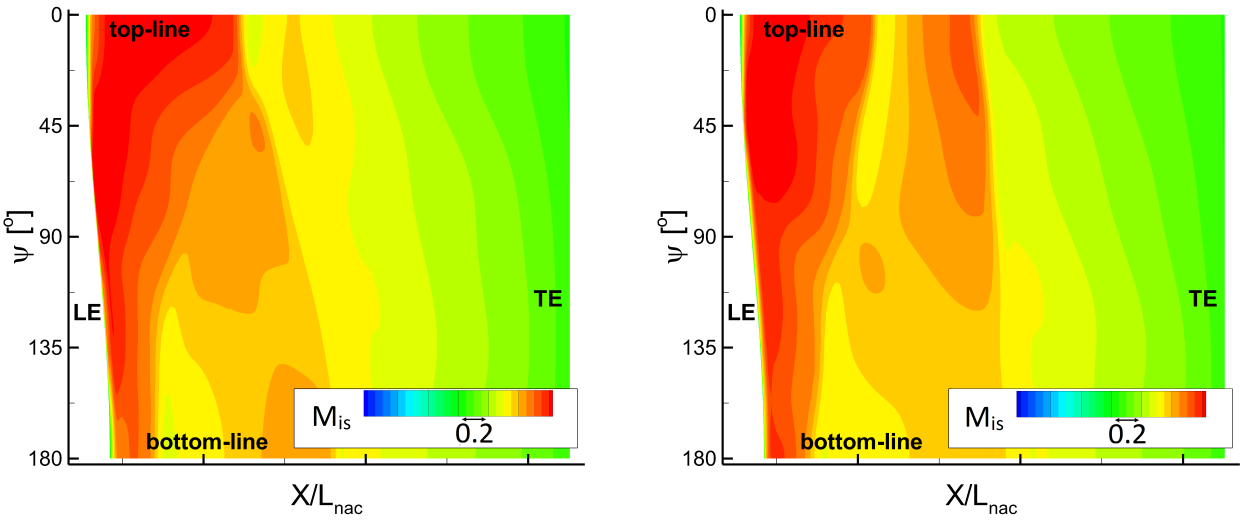

(a) Nacelle 1 **(b) Nacelle 2**

Fig. 5 Unwrapped nacelle aerodynamics for 2 samples in the training dataset, where LE refers to the nacelle trailing edge and TE to the trailing edge. The axial length of the nacelle surface changes with ψ due to the imposed intake scarf angle

along the nacelle surface. In this respect, the 3D geometry can be unwrapped in a 2D surface to help visualise the distributions. For example, Figure 5 shows the nacelle unwrapped surface of the 2 architectures that were presented in Figure 4. It is important to note that since the number of cells in the axial direction is constant for all the 3D geometries, their absolute location in the unwrapped surface changes. As such, low order models can not be directly trained in the unwrapped domain. For this reason, all the training data was interpolated in a Cartesian mesh with 1850 points. Overall, the ψ axis was discretised with 37 equidistant points, which equates to an azimuthal resolution of 5^o in the full 3D domain, and the X/L_{nac} axis was discretised with 50 equidistant points which was found to be sufficient to capture the main flow-physics associated with the peak isentropic Mach number, pre-shock isentropic Mach number and shock location. Having pre-processed all the data, the two different methods considered in this study for flow-field prediction were investigated (Sections II.A and II.B)

A. Training process

For the compiled database with 2000 nacelles samples, which provides a ratio between number of samples and degrees of freedom of $N_{samples}/N_s$ = 100, a range of ANNs were built to predict the isentropic Mach number on the aero-engine nacelles. The full-factorial combination of hyperpameters presented in Table 2 were considered to fine-tune the predictive accuracy of the low order model (Eq. 1). This resulted in the generation of 120 independent artificial neural networks. Based on the predictive accuracy with an independent database, the best performing ANN was downselected. The final metamodel was composed by 128 neurons per hidden layer, 2 hidden layers and the ReLu activation function. Based on the cross-validation with the independent set of 400 aero-engine nacelles, the root mean square error on the prediction of isentropic Mach number was RMSE = 0.019. Overall, it was found that the activation function has a large impact on the predictive accuracy, whereas ReLu consistently outperforms sigmoid and tanh. Similar findings were derived in previous studies in which artificial neural networks were used to predict nacelle drag [22].

For the method based on a combination of singular value decomposition and artificial neural networks, a key aspect is the number of eigenvalues of the matrix Σ (Eq. 3) that are used. This selection is typically based on the energy content that wants to be preserved. In the extreme case of preserving 100% of the energy content, i.e. all the modes are retained, this method for flow-field prediction would not present any advantage with respect to the previous approach because the dimensionality of the output would be the same. On the other hand, if a low number of modes are used with an associated low value of cumulative energy content, the SVD+ANN method would not viable for accurate predictions. As such, there is a clear trade-off between the achievable accuracy and overall dimensionality. For the training dataset with 2000 nacelles samples, the singular value decomposition method was used. Figure 6 presents the cumulative energy

(ϵ) of the eigenvalues of the matrix Σ as a function of the number of eigenvalues (s). As it is expected, there is an initial fast increment in ϵ as the value of s increases. Then, the cumulative energy asymptotically converges to 100%. The value of cumulative energy is directly linked to the accuracy in reconstructing the flow-field. For this training dataset, the root mean square error on the isentropic Mach number distribution as a function of the number of eigenvalues is presented in Figure 6. Different studies in the open literature use different values of cumulative energy to determine the number of modes used to reduce the dimensionality of the problem. For this work, a total number of 100 eigenvalues were used. These were the number of eigenvalues to retain 95% of the total energy content which had associated a root mean square error of approximately RMSE = 0.0055 (Figure 6). Having established the number of modes, the ANNs were trained with an output layer of 100 neurons (Figure 3). These neurons represent the coefficients of the matrix $\mathbf{V}^*$ (Eq. 3). As for the previous method, the full factorial combination of hyperparemeters presented in Table 2 was considered. To quantify the accuracy of the SVD+ANN approach, the isentropic flow-field along the aero-engine nacelle on the 400 unseen validation samples was prediced and the root mean square error calculated. Then, the best performing ANN was selected which resulted in final artificial neural network that was composed by 2 hidden layers, 64 neurons per hidden layer and the ReLu activation function. As previously, the activation function had a large impact on the model's accuracy. For this method, the the root mean square error of the validation dataset was RMSE = 0.022.

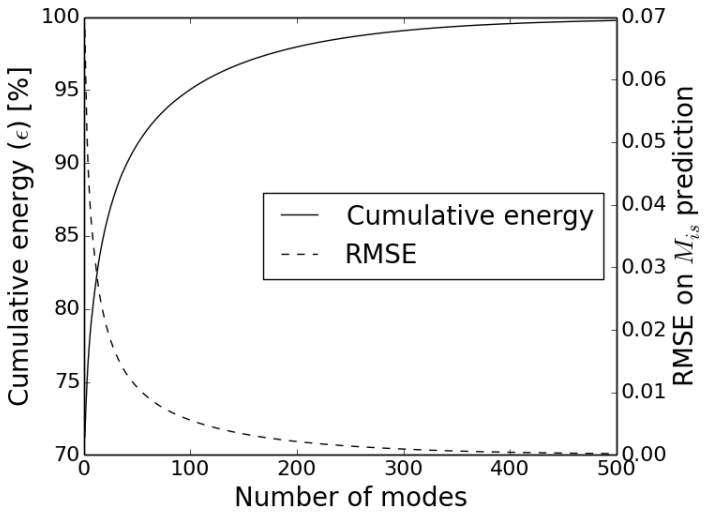

Fig. 6 Cumulative energy contents of the SVD modes and root mean square error on the prediction of M_{is}. Although there are 1850 modes, the range has been limited to 500 for visualization purposes

B. Qualitative and quantitative comparison between methods for flow-field prediction

Having trained the low order models for the two developed deep learning methods, flow-field prediction of aero-engine nacelles can be carried out. Figures 7 and 8 present two examples of aero-engine nacelles from the validation dataset in which the prediction of both methods are compared with CFD evaluations. For the first geometry (Figures 7), there is a strong shock wave at the nacelle top-line which is well predicted by both flow-field prediction methods. The shock location moves upstream as a function of the azimuthal location, which is also captured by both low order models. For the other configuration (Figure 8), there is an initial shock wave on the nacelle forebody and the flow reaccelerates to a second shock on the afterbody for azimuthal regions of $\psi > 45^o$. This flow topology is successfully captured by the ANN as well as the SVD+ANN approaches. Overall, there is a good qualitative agreement for both deep-learning architectures which highlights the possible suitability for preliminary nacelle design studies.

To provide a quantitative assessment on the accuracy of both models to capture the main flow characteristics of peak isentropic Mach number, pre-shock iseontropic Mach number and shock location, different azimuthal aero-lines ($\psi = 0^o$, $\psi = 90^o$ and $\psi = 180^o$ in Figure 1b) were extracted and compared with numerical simulations. This analysis is carried out for the configurations that were presented in Figures 7 and 8. For the first geometry (Figure 9), the methods of ANN and ANN+SVD are able to accurately predict peak and pre-shock isentropic Mach number and shock location in the top

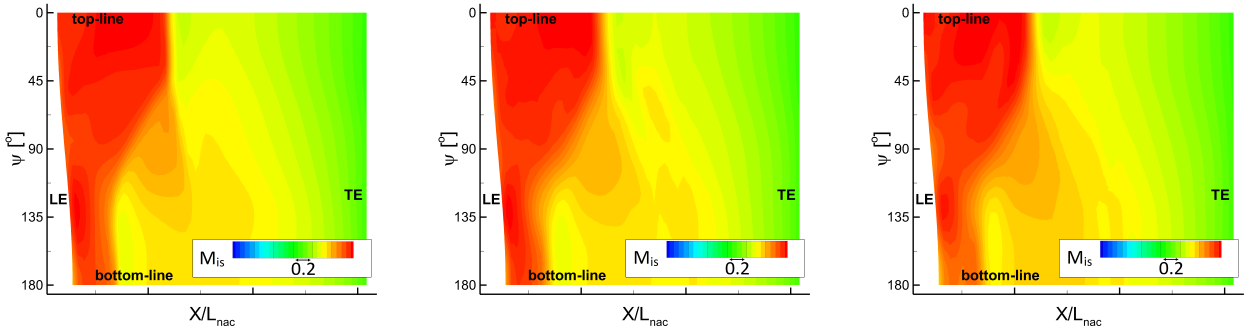

(a) CFD **(b) ANN prediction** **(c) SVD+ANN prediction**

Fig. 7 Flow-field prediction for Geometry-1 of the validation database

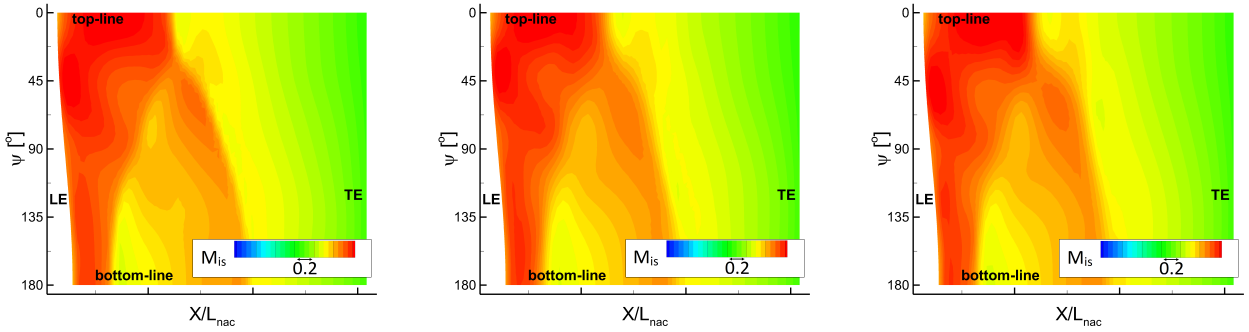

(a) CFD **(b) ANN prediction** **(c) SVD+ANN prediction**

Fig. 8 Flow-field prediction for Geometry-2 of the validation database

aero-line ($\psi = 0^o$) and bottom aero-line ($\psi = 180^o$). The predicted peak and pre-shock M_{is} are within $\Delta M_{is} = 0.015$ with respect to CFD. In addition, the shock location is within $\Delta X/L_{nac} = 0.01$. More differences appear for the side aero-line with $\psi = 90^o$ (Figure 9b). The ANN approach is able to predict the initial flow deacceleration that occurs at $X/L_{nac} \approx 0.2$ and the shock location that manifests at $X/L_{nac} \approx 0.38$. However, the method based on SVD+ANN fails to capture these flow characteristics and predicts a relatively smooth deceleration along the fancowl (Figure 9b). Similar analysis was carried out for the second geometry (Figure 10). Overall, both methods are able to predict the main flow characteristics that are simulated with CFD. For the top aero-line ($\psi = 0^o$), whilst the ANN approach has an excellent agreement in pre-shock M_{is} and shock location with respect to the numerical simulation, larger differences arise for the SVD+ANN method. Specifically, the pre-shock M_{is} is overpredicted by 0.08. For the other two aero-lines, i.e. $\psi = 90^o$ and 180^o, both predictions are in excellent agreement with CFD (Figure 10b and 10c).

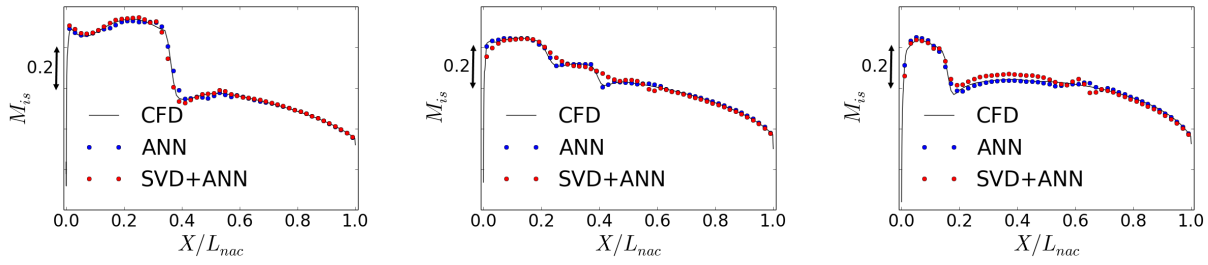

(a) $\psi = 0^o$ (top line) **(b) $\psi = 90^o$ (side line)** **(c) $\psi = 180^o$ (bottom line)**

Fig. 9 Isentropic Mach number comparison for different aero-lines of Geometry-1

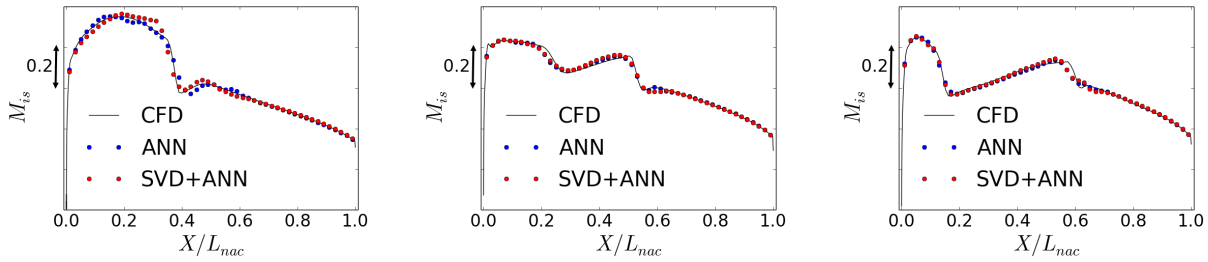

(a) ψ = 0^o (top line) **(b) ψ = 90^o (side line)** **(c) ψ = 180^o (bottom line)**

Fig. 10 Isentropic Mach number comparison for different aero-lines of Geometry-2

Based on the previous comparisons, the deep learning method based on ANN predicts more accurately the key transonic aspects of peak isentropic Mach number, pre-shock isentropic Mach number and shock location. Whilst the above is based only on two configurations, similar findings were identified across the full design space. To identify the regions along the nacelle with larger uncertainties, a statistical analysis of the predictive accuracy of M_{is} was performed. The M_{is} root mean square error (RMSE in Eq. 1) was calculated along the nacelle surface for the 400 nacelles evaluated in the validation database (Figure 11). The overall RMSE was 0.019 and 0.022 for the ANN and SVD+ANN approaches, respectively. It is important to note that the method that uses singular value decomposition and artificial neural networks (SVD+ANN) has a larger error on the top aero-line due to the difficulties of SVD+ANN to accurately predict shock waves [11] as showed in Figure 10a. Both approaches have an root mean square error in predicting M_{is} below 0.01 at the aft end of the nacelle due to the associated benign flow aerodynamics on that region (Figure 11). Based on this evidence, although both deep learning techniques have similar RMSE, it is recommended to use a surrogate model that is built directly with ANN and not with the combined SVD+ANN approach due to the capabilities of the ANN method to capture more accurately the shock-waves intensity and location.

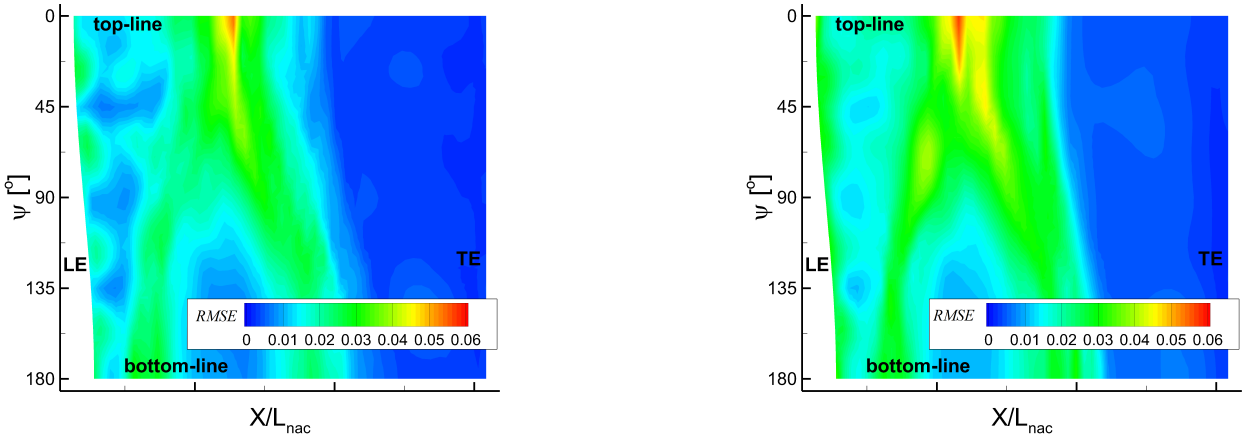

(a) ANN **(b) ANN+SVD**

Fig. 11 Statistical root mean square error (RMSE) in M_{is} prediction

To demonstrate the capability of the ANN method, the isentropic Mach number prediction along the nacelle for a range of configurations is presented in Figure 12. This is performed by doing perturbations of the top aero-line with respect to a baseline geometry. For this purpose, the key design variables of f_{max} and r_{max} are changed (Figure 1a). Relative to the baseline geometry with the lowest values of f_{max} and r_{max} (Figure 12), there are significant changes on the flow characteristics across the design space. For example, increasing the top-line maximum radius at fixed f_{max} results in a downstream movement of the shock from X/L_{nac} = 0.37 to X/L_{nac} = 0.45. In addition, relative to the baseline with a well-defined single shock on the top aero-line, a double shock pattern generates as f_{max} is increased. Subsequently, the strength of the second shock is greater with larger values of r_{max}.

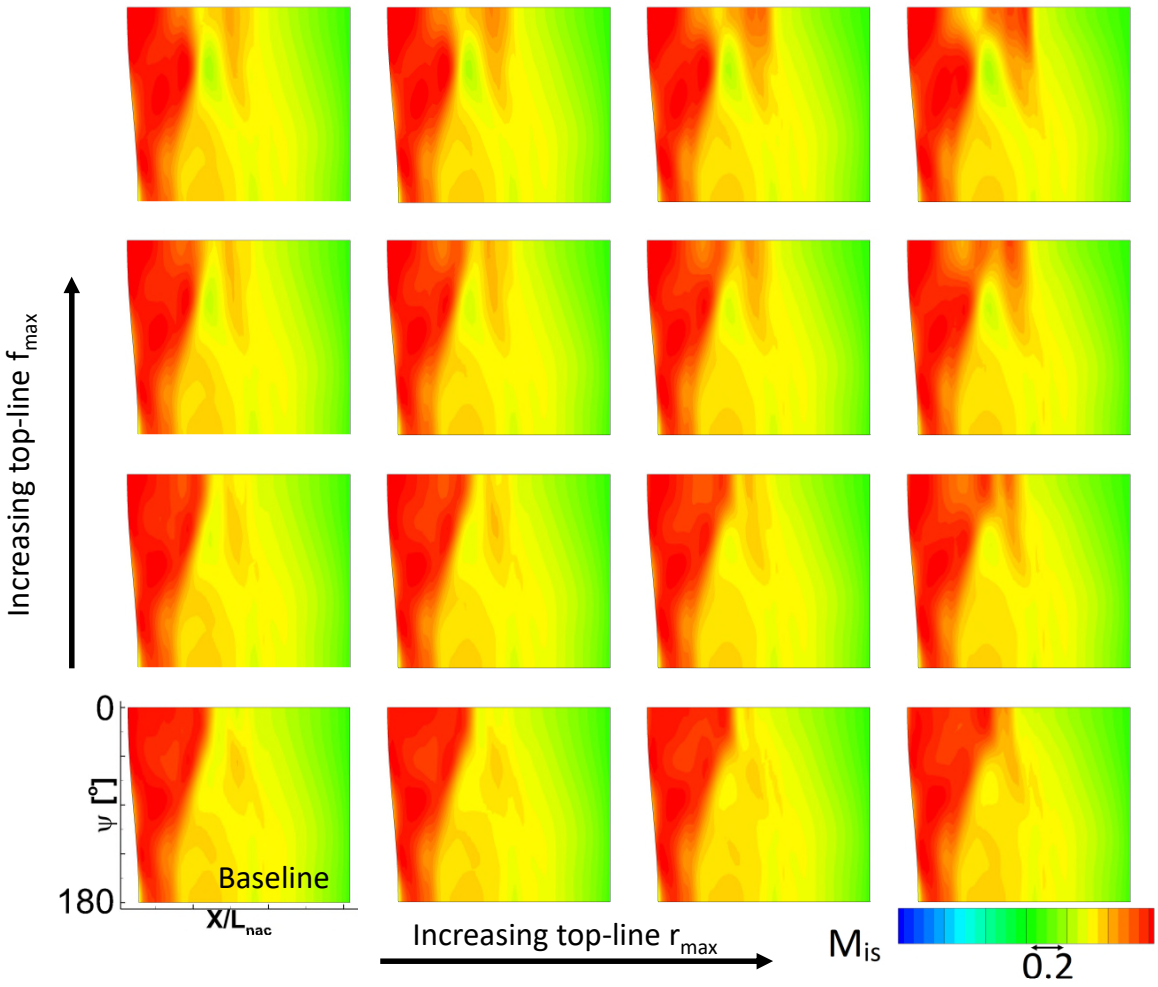

Fig. 12 Deployment of the ANN method for predictions of flow-field across the design space

IV. Conclusion

Two different methods for flow-field prediction in transonic applications have been investigated. They are based on artificial neural networks (ANN), and a combination of singular value decomposition and ANN. Both approaches have been tested for 3D compact civil aero-engine nacelles. The methods present a similar root mean square error on the prediction of the isentropic Mach number along the nacelle. However, it is demonstrated that the ANN approach is more accurate to capture the peak isentropic Mach number, pre-shock isentropic Mach number and shock location. Based on these findings is suggested to use the ANN approach for future flow-field prediction studies at transonic conditions. This work has also demonstrated the capabilities of the developed ANN method to map out the flow characteristics across the design space. This can be very useful to provide design guidelines within a multi-disciplinary design and optimisation environment. Future work will build on this new capability to consider aerodynamic and aero-structural requirements during the design process.

Acknowledgments

This project has received funding from the Clean Sky 2 Joint Undertaking (JU) under grant agreement number 101007598. The JU receives support from the European Union's Horizon 2020 research and innovation programme and the Clean Sky 2 JU members other than the Union.

Data availability statement

Due to commercial confidentiality agreements the supporting data are not available.

References

[1] Sobester, A., and Powell, S., "Design space dimensionality reduction through physics-based geometry re-parameterization," *Optimization and Engineering*, Vol. 14, 2013, pp. 37–59.

[2] Shah, H., Hosder, S., Koziel, S., Tesfahunegn, Y. A., and Leifsson, L., "Multi-Fidelity Robust Aerodynamic Design Optimization under Mixed Uncertainty," *Aerospace Science and Technology*, Vol. 45, 2015, pp. 17–29.

[3] Viquerat, J., and Hachem, E., "A supervised neural network for drag prediction of arbitrary 2D shapes in laminar flows at low Reynolds number," *Computers and Fluids*, Vol. 15, 2020, p. 104645.

[4] Du, X., He, P., and Martins, R., "Rapid airfoil design optimization via neural networks-based parameterization and surrogate modeling," *Aerospace Science and Technology*, Vol. 113, 2021, p. 106701.

[5] Sevant, N. E., Bloor, M. I. G., and Wilson, M. J., "Aerodynamic Design of a Flying Wing Using Response Surface Methodology," *Journal of Aircraft*, Vol. 37 (4), 2000, pp. 562–569.

[6] Venturelli, G., and Benini, E., "Kriging-assisted Design Optimization of S-Shape supersonic compressor cascades," *Aerospace Science and Technology*, Vol. 58, 2016, pp. 275–297.

[7] Sabater, C., Sturmer, P., and Bekemeyer, P., "Fast Predictions of Aircraft Aerodynamics Using Deep-Learning Techniques," *AIAA Journal*, Vol. 60, No. 9, 2022, pp. 5249–5261.

[8] Duchon, J., "Splines minimizing rotation-invariant semi-norms in Sobolev spaces," *Constructive Theory of Functions of Several Variables, Part of the Lecture Notes in Mathematics book series*, Vol. 571, 2006, pp. 85–100.

[9] Qamar, A., and Sanghi, S., "Steady Supersonic Flow-Field Predictions using Proper Orthogonal Decomposition Technique," *Computer & Fluids*, Vol. 38, 2009, pp. 1218–1231.

[10] McCaslin, J. O., Courtine, E., and Desjardins, O., "A Fast Marching Approach to Multidimensional Extrapolation," *Journal of Computational Physics*, Vol. 274, 2014, pp. 393–412.

[11] Li, J., and Zhang, W., "The Performance of Proper Orthogonal Decomposition in Discontinuous Flows," *Theoretical and Applied Mechanics Letters*, Vol. 6, 2016, pp. 236–243.

[12] Birch, N., "2020 Vision: The Prospects for Large Civil Aircraft Propulsion," *The Aeronautical Journal*, Vol. 104 (1038), 2000, pp. 347–352.

[13] Goulos, I., MacManus, D., Hueso-Rebassa, J., Tejero, F., Au, A., and Sheaf, C., "Impact of Installation on the Performance of an Aero-Engine Exhaust at Wind-Milling Flow Conditions," *ASME TurboExpo 2023, GT2023-100833*, 2023.

[14] Tejero, F., MacManus, D., Matesanz-Garcia, J., Swarthout, A., and Sheaf, C., "Towards the Design and Optimisation of Future Compact Aero-Engines: Intake/Fancowl Trade-Off Investigation," *International Journal of Numerical Methods for Heat & Fluid Flow*, 2022.

[15] Silva, V. T., Lundbladh, A., Petit, O., and Xisto, C., "Multipoint Aerodynamic Design of Ultrashort Nacelles for Ultrahigh-Bypass-Ratio Engines," *Journal of Propulsion and Power*, Vol. 0, 2022, pp. 1–18.

[16] Lamkin, A., Yildirim, A., and Martins, J., "Coupled Aeropropulsive Analysis and Optimization of a High Bypass Turbofan Engine," *33rd Congress of the International Council of the Aeronautical Sciences (ICAS 2022*, 2022.

[17] Tang, Z., Zhang, M., and Hu, X., "Optimal Shape Design and Transition Uncertainty Analysis of Transonic Axisymmetric Natural Laminar Flow Nacelle at High Reynolds Number," *Aerospace Science and Technology*, Vol. 121, 2012, p. 107345.

[18] Heidebrecht, A., and MacManus, D., "Surrogate Model of Complex Non-Linear Data for Preliminary Nacelle Design," *Aerospace Science and Technology*, Vol. 84, 2019, pp. 399–411.

[19] Song, W., and Keane, A. J., "Surrogate-Based Aerodynamic Shape Optimization of a Civil Aircraft Engine Nacelle," *AIAA Journal*, Vol. 45, 2007, pp. 2565–2574.

[20] Fang, X., Zhang, Y., Li, S., , and Chen, H., "Transonic Nacelle Aerodynamic Optimization Based on Hybrid Genetic Algorithm," *17th AIAA/ISSMO Multidisciplinary Analysis and Optimization Conference, AIAA AVIATION Forum, AIAA Paper Number 2016-3833*, 2016.

[21] Yao, Y., Ma, D., Yang, M., Zhang, L., and Guo, Y., "Adaptive-Surrogate-Based Robust Optimization of Transonic Natural Laminar Flow Nacelle," *Chinese Journal of Aeronautics*, Vol. 34, 2021, pp. 36–52.

[22] Tejero, F., MacManus, D., Sanchez-Moreno, F., and Sheaf, C., "Neural Network-Based Multi-Point, Multi-Objective Optimisation for Transonic Applications," *Aerospace Science and Technology*, Vol. 136, 2023, p. 108208.

[23] Sanchez-Moreno, F., MacManus, D., Hueso-Rebassa, J., Tejero, F., J.Matesanz-Garcia, and Sheaf, C., "Optimization of Installed Compact and Robust Nacelles Using Surrogate Models," *Proceedings of 33rd Congress of the International Council of the Aeronautical Sciences*, 2022.

[24] Tejero, F., MacManus, D., Hueso-Rebassa, J., Sanchez-Moreno, F., Goulos, I., and Sheaf, C., "Aerodynamic Optimisation of Future Civil Aero-Engines by Dimensionality Reduction and Multi-Fidelity Techniques," *International Journal of Numerical Methods for Heat & Fluid Flow*, 2022.

[25] Sanchez-Moreno, F., MacManus, D., Tejero, F., J.Matesanz-Garcia, and Sheaf, C., "Robustness of Optimisation Algorithms for Transonic Aerodynamic Design," *Proceedings of 9th European Conference for Aeronautics and Space Sciences, EUCASS-3AF*, 2022.

[26] Christie, R., Robinson, M., Tejero, F., and MacManus, D., "The Use of Hybrid Intuitive Class Shape Transformation Curves in Aerodynamic Design," *Aerospace Science and Technology*, Vol. 95, 2019, p. 105473.

[27] Matesanz-Garcia, J., Piovesan, T., and MacManus, D., "Aerodynamic Optimization of the Exhaust System of an Aft-Mounted Boundary Layer Ingestion Propulsor," *International Journal of Numerical Methods for Heat & Fluid Flow*, 2022.

[28] Tejero, F., MacManus, D., and Sheaf, C., "Impact of Droop and Scarf on the Aerodynamic Performance of Compact Aero-Engine Nacelles," *AIAA SciTech 2020 Forum and Exposition, AIAA Paper 2020-1522*, 2020.

[29] Swarthout, A., MacManus, D., Tejero, F., Matesanz-García, J., Boscagli, L., and Sheaf, C., "A Comparative Assessment of Multi-Objective Optimisation Methodologies for Aero-Engine Nacelles," *33rd Congress of the International Council of the Aeronautical Sciences (ICAS)*, 2022.

[30] *ANSYS FLUENT User's Guide*, Ansys Inc., 275 Technology Drive, Canonsburg, PA 15317, ????

[31] Menter, F. R., "Two-Equation Eddy-Viscosity Turbulence Models for Engineering Applications," *AIAA Journal*, Vol. 32, No. 8, 1994, pp. 1598–1605.

[32] Helton, J. C., and Davis, F. J., "Latin Hypercube Sampling and the Propagation of Uncertainty in Analyses of Complex Systems," *Engineering and System Safety*, Vol. 81, 2003, pp. 23–69.

[33] Schreiner, B. D. J., Tejero, F., MacManus, D., and Sheaf, C., "Robust Aerodynamic Design of Nacelles for Future Civil Aero-Engines," *Proceedings of ASME Turbo Expo 2020: Turbomachinery Technical Conference and Exposition, GT2020-14470*, 2020.

https://dspace.org/

Deep-learning for flow-field prediction of 3D non-axisymmetric aero-engine nacelles

Tejero, Fernando; MacManus, David G.; Matesanz García, Jesús; Boscagli, Luca; Hueso Rebassa, Josep ...

2023-06-08
American Institute of Aeronautics and Astronautics (AIAA)
https://doi.org/10.2514/6.2023-3307
Tejero F, MacManus DG, Matesanz García J, et al., (2023) Deep-learning for flow-field prediction of 3D non-axisymmetric aero-engine nacelles. In: 2023 AIAA Aviation and Aeronautics Forum and Exposition (AIAA AVIATION Forum), 12-16 June 2023, San Diego, USA. Paper number AIAA 2023-3307

Downloaded from a DSpace repository. https://dspace.org/